

Experimental and numerical analysis of pure aluminium shear panels for seismic protection of structures: An overview

G. De Matteis¹, G. Brando¹, F.M. Mazzolani²

¹Dept. of Engineering, University of Chieti-Pescara "G. D'Annunzio", Italy

²Dept. of Structural Engineering, University of Naples "Federico II", Italy

Among several types of metal-based devices conceived as dampers for the seismic protection of new and existing structures, shear panels represent a valid system. Recently, a research aimed at investigating the use of aluminium to develop new devices for passive protection has been performed by the authors. Shear panels made of pure aluminium and suitably reinforced by ribs to delay shear buckling in the plastic deformation field, have been tested and numerically analysed. Two different panel typologies have been taken into account. The former one, conceived in a full bay configuration, has in-plane dimensions of 1500x1000 mm² and a thickness of 5 mm, whereas the latter is obtained by means of stiffened bracing type pure aluminium shear panels with a square shape with side length of 500 mm and 5 mm of thickness. Several types of slenderness ratios of the ribs have been considered, in order to evaluate the influence on the cyclic performance of the system. In the current paper a wide overview on the most recent results of the above research is provided and discussed to point out the good structural performance in terms of strength, stiffness and dissipative capacity of the proposed device.

Keywords: Aluminium alloy, cyclic tests, FEM, numerical models, dissipative devices, low yield stress material, shear panels, buckling curves of stiffened plates

1 Introduction

Recent strong earthquakes urged researches and engineers to design new buildings, as well as to retrofit existing structures, by using new technologies based on the employment of devices characterized by a suitable dissipative capacity.

As a consequence protection of structures by using special devices acting as hysteretic and/or visco-elastic dampers becomes today a valuable approach to prevent seismic damage of steel and reinforced concrete buildings. Basically, the earthquake input energy

is directed towards these special elements protecting the primary members of the structures for plastic deformations. In this way, damages of beams, columns and joint could be even completely avoided also after strong seismic shocks [Christopoulos and Filiatrault, 2006].

In this framing, it was proved that low yield stress point metal shear panels are a valid system, thanks to the shear dissipative mechanism they are able to guarantee, also for a limited deformation demand [Nakashima et al., 1994; De Matteis et al., 2007]. This system allows the plastic deformation to be spread throughout the entire surface of the device, rather than concentrate it in a limited area as occurs for many other dissipative elements commonly used for adding structural damping.

In the last ten years, a significant research activity on pure aluminium devices has been carried out by the authors. In particular shear panels made of pure aluminium and suitably reinforced by ribs in order to delay shear buckling in the plastic deformation field, have been tested and numerically analysed.

The implemented research has been carried out on three different levels.

The first level has focused on the material behaviour. The used alloy presents many innovative aspects that need to be analysed in order to interpret correctly the mechanical behaviour under both monotonic/cyclic and static/dynamic loading. Since it is not possible to get a 100% pure aluminium, an almost pure aluminium, namely the alloy EN AW 1050A, has been used. Moreover, in order to improve the mechanical features of the material, a special heat treatment, consisting in an annealing, has been carried out. The choice of pure aluminium as base material was justified by both the low yield strength and high ductility that it is able to offer. In fact the proposed alloy is characterised by a very low strength (conventional 0.2% strain rate stress equal to about 18 MPa after heat treatment), high hardening, large ductility and low specific weight.

The second and third levels of the research concern the cyclic behaviour of shear panels. Two different panel typologies have been taken into account by developing both experimental and numerical studies. The first panel typology, conceived for application in framed structure with a full bay configuration, had in-plane dimensions 1500 x 1000 mm² and a thickness of 5 mm; the second panel typology had a square shape with side lengths of 500 mm and a thickness of 5 mm. In both cases several types of plate slenderness ratios have been tested in order to evaluate their influence on the cyclic performance of system. The obtained results have been used as basis for the calibration of numerical models as well as to interpret the influence of the applied ribs on the structural performance of the tested systems.

In the following an overview of the most significant results of the above described research is provided and discussed.

2 The adopted material: heath treatment and mechanical features

2.1 *Material heath treatment*

Generally, impurities in pure aluminium generates dislocations at atomic level provoking a hardening effect. This causes an increase of the conventional 0.2% strain rate stress $f_{0.2}$ of the material (for the proposed material about 100MPa versus 30 MPa) and a heavy reduction of ductility (strain limits for the proposed material is about 5% versus 40%) with respect to the nominal values. In particular, crystallographic planes assume a bended doubled shape characterized by the fact that atoms are forced in an asymmetric position in the basic crystal lattice. This entails an increase of the internal energy associated to the rising of macroscopic residual stresses, known as Heyn stresses, characterized by a random distribution [Pansieri, 1957]. The same effects are also produced by the “transformation percentage rate” (see Pansieri, 1957, as well), which strongly relies on the ratio between the thicknesses of the initial aluminium block that has to be worked and the one of the final plate after the manufacturing process.

A proper annealing may produce the softening of the base material, with the annulment of existing microscopic and macroscopic residual stresses, providing the primitive plasticity to the material. Three different structural transformations are produced on the crystal lattice by annealing: (i) the crystal recovery, (ii) the re-crystallization and (iii) the enlargement of the grains.

In Figure 1 these phenomena, which arises in the heating phases when temperature grows, are schematically described. It is evident that the diminishing of residual stresses associated to the enlargement of the grains provokes a significant lowering of the elastic strength of the base material. The same effect is obtained for the ultimate strength.

Furthermore the re-crystallization interval varies with the initial hardening grade of the annealed metal, which is completely erased at the final state.

In Figure 2a, the average stress-strain curves for the adopted materials obtained from different tests before and after the heat treatment are depicted. It is worth noticing that the same heat treatment produced different results for another alloy tested for comparison. In particular, the effect of heath treatment was less important in case of aluminium AW 5154A, for which, even if the conventional yield strength f_{02} of heat treated alloy was halved with respect to the not treated material, the ultimate strain ϵ_i remained almost

unchanged due to the higher content of alloying elements. On the other hand, it is apparent that the heat treated aluminium alloy AW 1050A is very suitable for the application under consideration. In fact, in this case the yield strength was reduced to one/tenth the one offered by the non treated alloy. In addition ductility increased considerably.

2.2 Monotonic and cyclic behaviour under static loading

On the basis of experimental tests carried out on a large number of specimen made of heat treated AW1050 alloy an initial tangent elastic modulus $E = 66666$ MPa, a proportionality stress $f_{0.01} = 7.12$ MPa and a conventional yielding stress $f_{0.2} = 19.12$ MPa have been

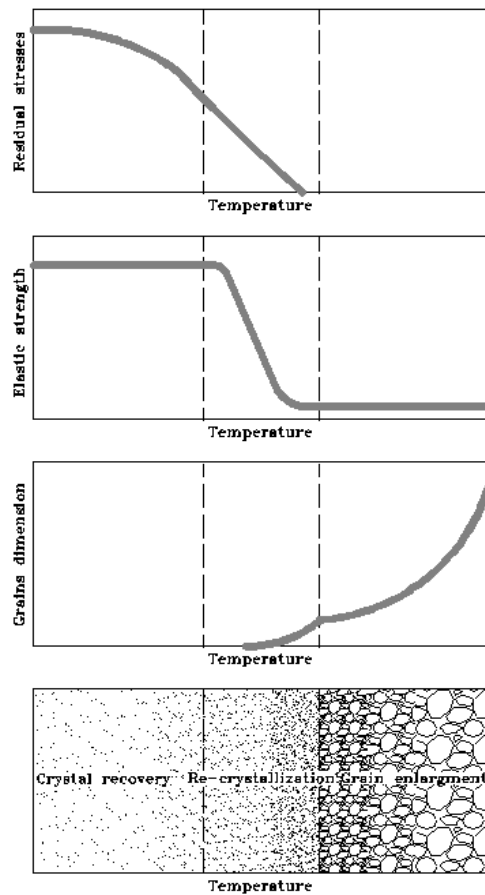


Figure 1. Schematic representation of the annealing phases in hardened metals with increasing temperature

measured [De Matteis et al., 2008^a]. For specimens that failed within the extremes of the extensometer, a ductility ϵ_u varying in the range of 30-40% has been observed. The obtained results allowed to find a proper analytical relationship able to fit the observed behaviour. On this purpose, an initial screening among the most reliable material models available in literature for aluminium alloys has been carried out. In particular, it has been observed that the Ramberg-Osgood law [1943] calibrated by using the two conventional stresses corresponding to residual strains of 0.1% ($f_{0.1}$) and 0.2% ($f_{0.2}$) is not

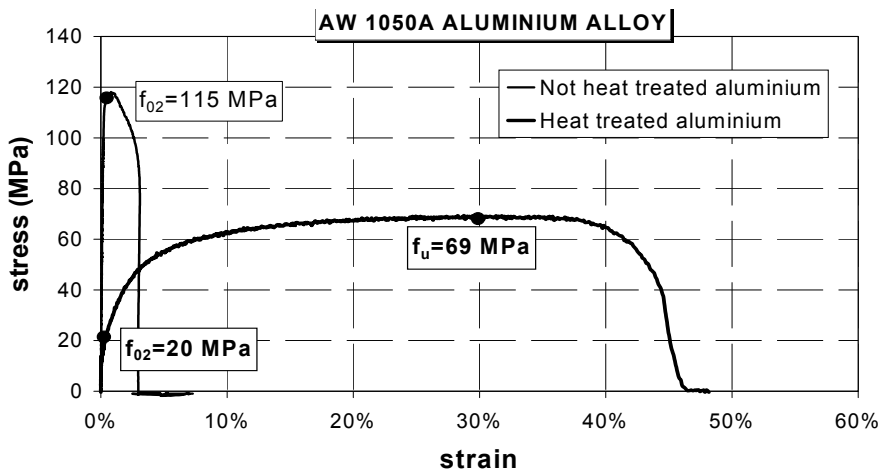


Figure 2a. Average stress-strain curves of the adopted alloy

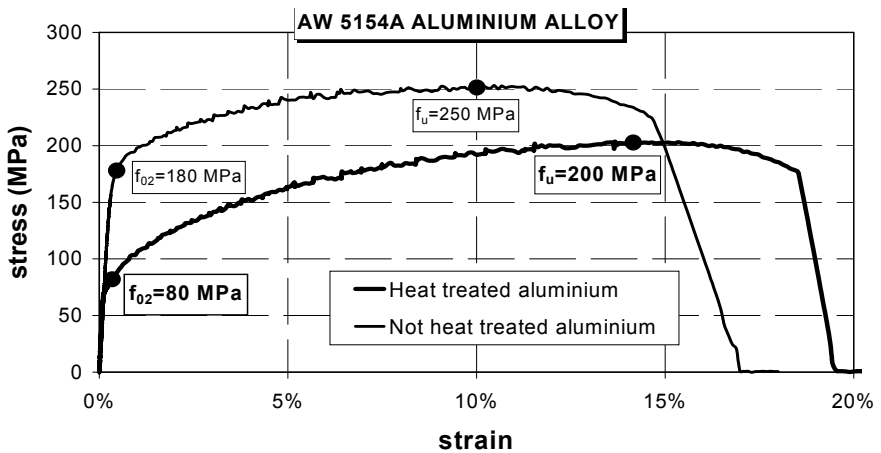


Figure 2b. Average stress-strain curves of the AW5154A alloy before and after the applied heat treatment process.

able to reproduce the material behaviour, as the material hardening, and therefore also the ultimate stress, is not appropriately modelled (see Figure 3). Also, the stress-strain model proposed by Baehre [1966] is able to suitably reproduce the proportional and elastic behaviour of the material, but not to adequately fit the “knee” of the curve obtained by experimental tests. Nevertheless, considering that Baehre’s law is expressed by dividing the strains domain in three different branches and by assigning a distinctive expression for each branch, a proper analytical law of the experimental curve has been obtained by unchanging the first two branches of the model and replacing the third branch with two relationships expressly calibrated on the basis of the available experimental results (Fig. 3). The analytical expression of this relationship is detailed in [De Matteis et al., 2008^a].

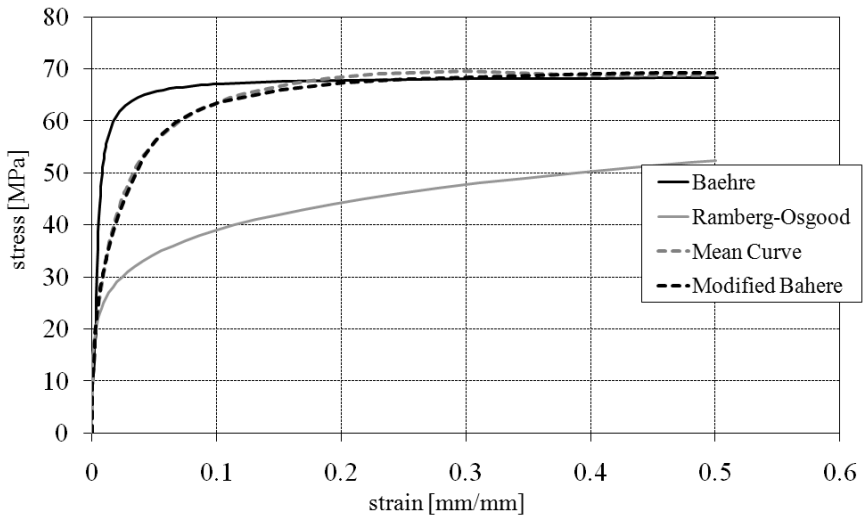


Figure 3. Application of existing material models to heat treated aluminium alloy EN-AW 1050A H24

In order to characterise the hysteretic behaviour of the material, as for such kind of strong hardening materials the isotropic hardening component may have a significant effect producing the enlargement of the hysteretic cycles, tensile-compression cyclic tests on pure aluminium specimens have been carried out. For this purpose, the testing specimens were equipped with a steel “jacket” able to inhibit out-of-plane deformations due to buckling phenomena in compression (Fig. 4a).

The obtained results have shown a very good cyclic behaviour (Fig. 4b) characterized by full hysteretic cycles, a substantial iso-resistance for each displacement level, or rather the same tensile-compression values for each displacement demand, and the existence of a

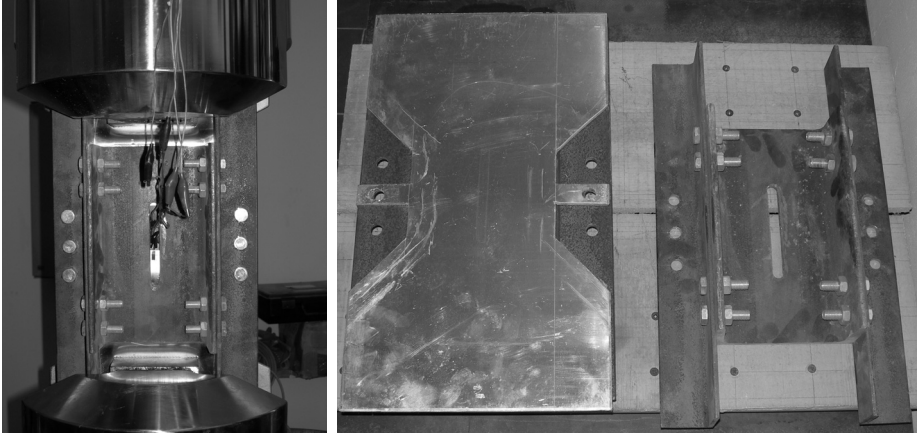


Figure 4a. Tested buckling inhibited specimen

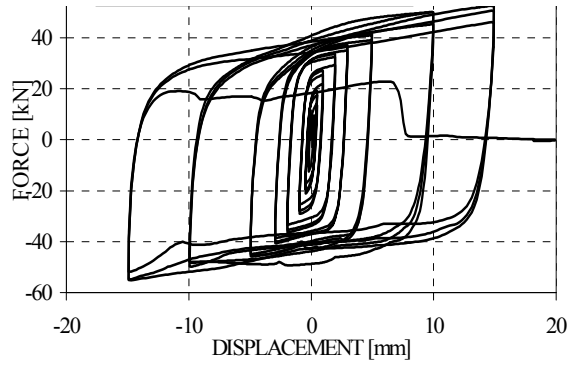


Figure 4b. Hysteretic behaviour of the buckling inhibited specimens

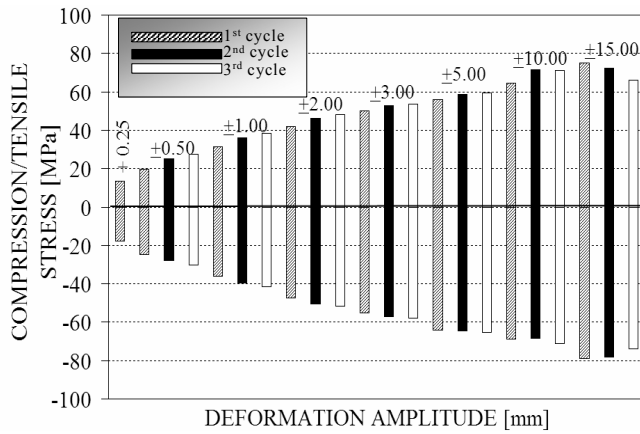


Figure 4c. Strength cycles of the buckling inhibited specimens

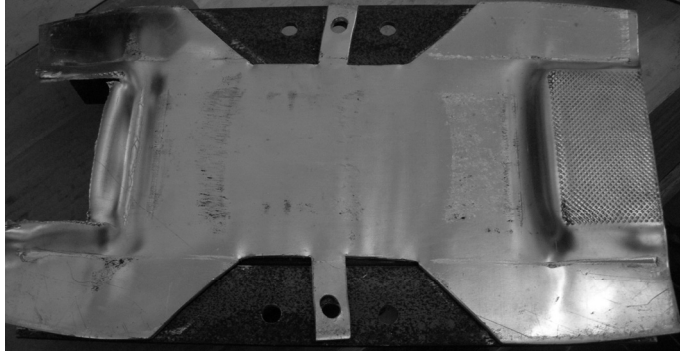


Figure 4d. Collapse mode of the buckling inhibited specimens

isotropic hardening component (Fig. 4c). As far as the cyclic degradation is concerned, the performed tests did not allow to yield a final conclusion, as the testing specimens revealed unexpected local buckling phenomena, which invalidated the results for displacements higher than +15 mm (Fig. 4d).

In order to model the cyclic behaviour of the base material, defined in terms of both kinematic and isotropic hardening, a numerical simulation of the above cyclic experimental test has been carried out. In the numerical model, which is shown in Figure 5a for the maximum value of Mises stresses, the specimen has been restrained at the

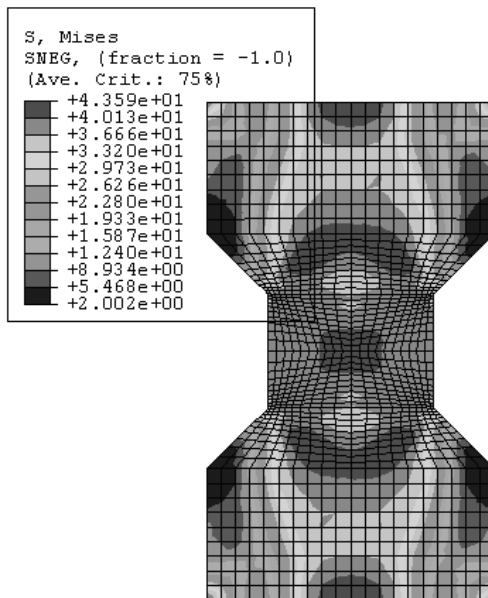


Figure 5a. Simulation model used in calibration of the material hardening

bottom edges by constraining the relevant points to a pinned external reference point. Then, a uniform load has been applied on the upper specimen edge according to the performed experimental test. Also, the confining boundary action exerted by the steel jacket, which inhibits the out-of-plane deformations of the testing sample, has been modelled by fixing this motion component for the whole specimen surface. The kinematic hardening component has been calibrated directly as a half-cycle curve obtained from monotonic tests, assuming plastic deformations starting from a proportional stress value

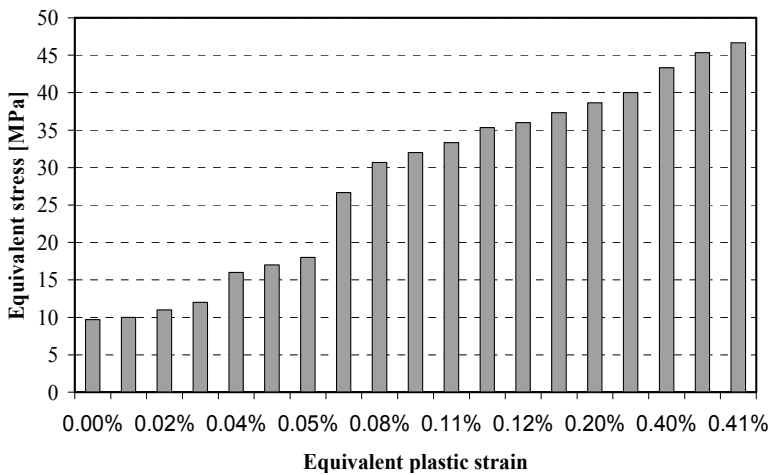


Figure 5b. Isotropic hardening component used in calibration of the material hardening

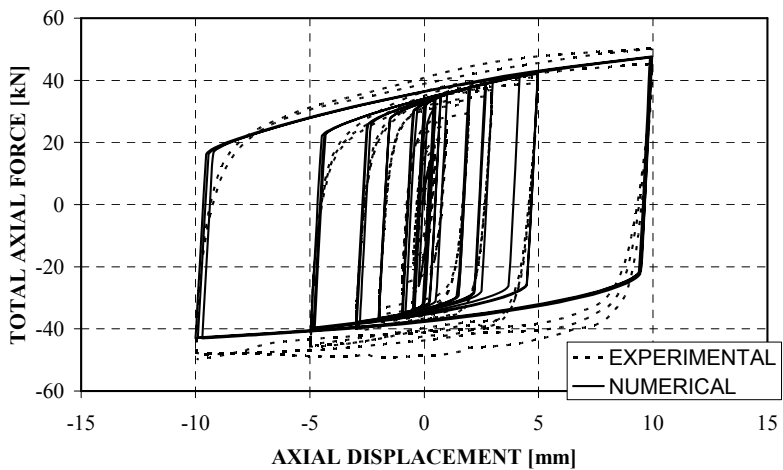


Figure 5c. Comparison between experimental and numerical results used in calibration of the material hardening

$f_y = 9.76$ MPa. On the other hand, the isotropic component has been determined as a result of a trial and error procedure, whose final response is reported in Figure 5b in terms of “equivalent stress-equivalent plastic strain” relationship. The comparison between the experimental and numerical results, which is illustrated in Figure 5c in terms of hysteretic cycles, shows that the numerical implemented modelling of the base material is reliable and useful to be adopted for the numerical simulation of the whole aluminium shear panel.

2.3 Monotonic behaviour under dynamic loading

In order to detect the influence of the strain rate on the main mechanical features of the proposed material, a study on its dynamic response has been carried out for different load velocity levels. For this purpose, eleven axis-symmetric notched specimens (Fig. 6) have been tested at different rates, using a Servo-hydraulic machine, for medium-low velocity value, and a Split Hopkinson Tension Bar (SHTB) for high imposed rates. The tests have

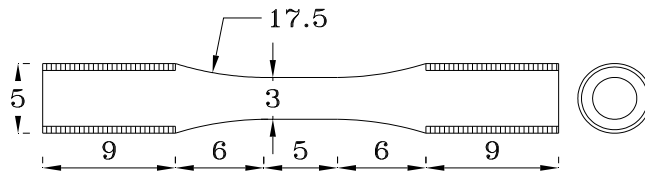


Figure 6. Geometry of the tested notched specimens (dimensions in mm)

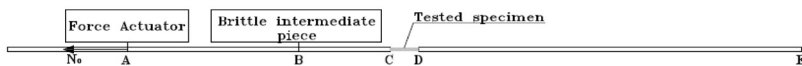
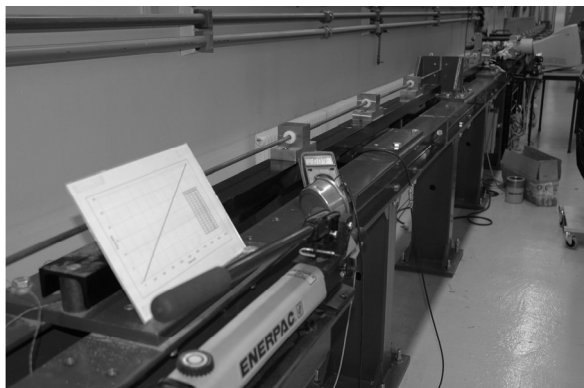


Figure 7. The Split Hopkinson Tension Bar used for strain-rate tests

been carried out at the SIMLAB of the University of Thronheim (Norway) NTNU (Fig. 7). Among the tested notched specimens, only seven have provided significant results (shown in Figure 8a in terms of stress-strain curves), as the others have been invalidated by the fact that they have been tested for strain rate values of around $1.2E2 \text{ s}^{-1}$. This represents a lower threshold under which the propagated elastic wave in the output bar is reflected in point E and goes across the specimen before that it is able to reach an equilibrium state and therefore its failure.

For intelligibility, in Figure 8a, the curve obtained for a specimen tested under a strain rate of $1.13E2 \text{ s}^{-1}$ is also depicted, proving the untrustworthiness with respect to the other curves corresponding to other rate values.

In Figure 8b the specimen within the input and the output bars before and after test is depicted, whereas in Figure 8c the typical failure mode of each specimen is shown in order that it can be taken as a reference for future numerical modelling.

It is evident that the conventional yield stress is more sensitive to rate changes, than the ultimate strength as the former reveals variation of 335%, while the latter shows a maximum increase of 39%. Further it can be noticed that the increase of the applied strain rate produces a reduction of the material ductility of around 29%.

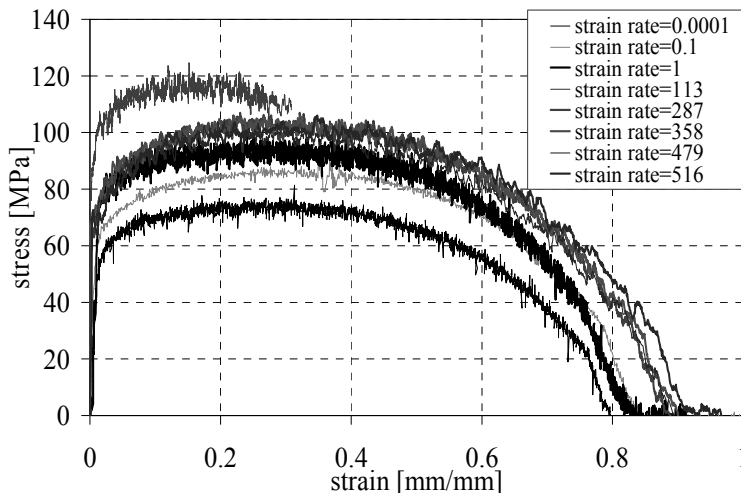


Figure 8a. Stress-strain relationships for different strain rates of the dynamic tests

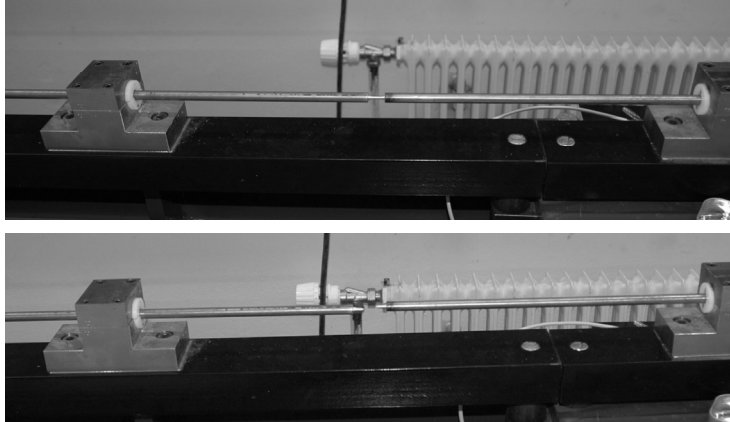


Figure 8b. Specimen in the SHTB before and after the dynamic tests.

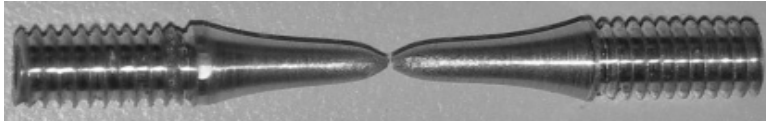


Figure 8c. Typical failure mode during the dynamic tests

3 Analysis of full bay shear panels

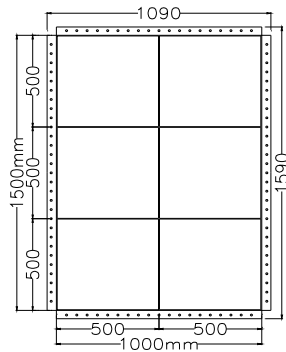
3.1 Experimental tests

Experimental tests were carried out on panel specimens measuring 1500 by 1000 mm² and a thickness of 5 mm. They were stiffened with longitudinal and transversal ribs made with either open rectangular shaped stiffeners with a depth of 60 mm, obtained by the same sheeting used for the base shear plate, or steel channel shape. In the former case the stiffeners were connected to the shear plate by a welding process (MIG), whose influence on the basic material is given in De Matteis et al. (2010), while in the latter case bolted joints were used.

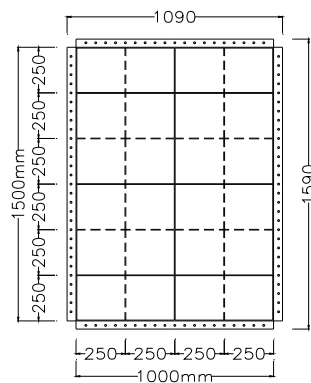
In the experimental programme, four different types of panel configurations were considered, presenting different geometry of the applied ribs (see Figure 9, where the adopted nomenclature for each specimen is also shown). For panel type B, ribs were placed on both sides of the plate according to a square field of 500 mm side length. Contrarily, panel configuration type F was stiffened with ribs alternatively placed on the two sides of the plate in order to obtain square fields of 250 mm of side length and to balance the out-of-plane deflection induced by the welding process. Panels with configuration type G and

H were successively designed in order to overcome some drawbacks pointed out in the first cyclic tests carried out on panels type B and F [De Matteis et al., 2007^a, De Matteis et al., 2008^b]. In detail, for each of them ribs have been placed in order to realize fields of 250 mm of side length, but contrarily to panel F, they have been arranged on the two faces of the panels in the same position. Further, welded and bolted ribs have been used for panel type G and H respectively.

As a consequence, the internal fields of the tested shear panels were characterised by different slenderness ratios, namely $b/t=100$ for panel type B and $b/t=50$ panel type F. Panel type G was characterized by $b/t=50$, but such a reduced slenderness ratio was of $b/t=25$ in the corners of the panels. Moreover, contrarily to Panel type F, Panel type G presented the same stiffener arrangement on the two faces. Panel type H was characterized by $b/t=50$,



panel type B ($b/t=100$)



panel type F ($b/t=50$)

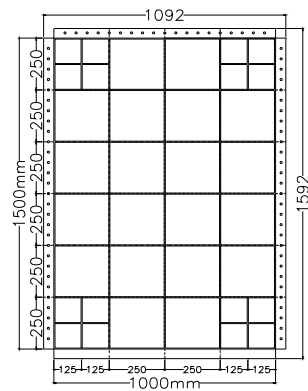
Figure 9. Geometrical configuration of tested specimens

having a configuration similar to panel type F, but it was ribbed by means of steel channels (UPN50). This choice arose from the necessity to eliminate the geometrical and mechanical imperfections induced by the welding process of stiffeners.

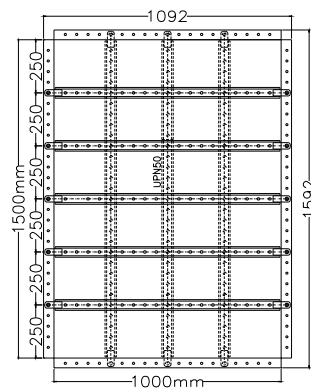
The shear load on the panels was applied by means of a pin-jointed steel frame composed by very rigid members and equipped with lateral out-of-plane braces (Fig. 10a).

The external load was applied at the top beam of the frame by means of a servo-hydraulic actuator (MTS System Corporation), characterised by a range of displacement of ± 250 mm and a load capacity of 500 kN in compression and 300 kN in tension. The actuator was connected to a very rigid lateral support steel frame used as reaction frame (Fig. 10b).

The specimens were connected to the loading steel frame by steel cover plates with friction high-strength grade 8.8 steel bolts, having a diameter of 14 mm and with a pitch of 50 mm



panel type G ($b/t=50-25$)



panel type H ($b/t=100$)

Figure 9. Continued

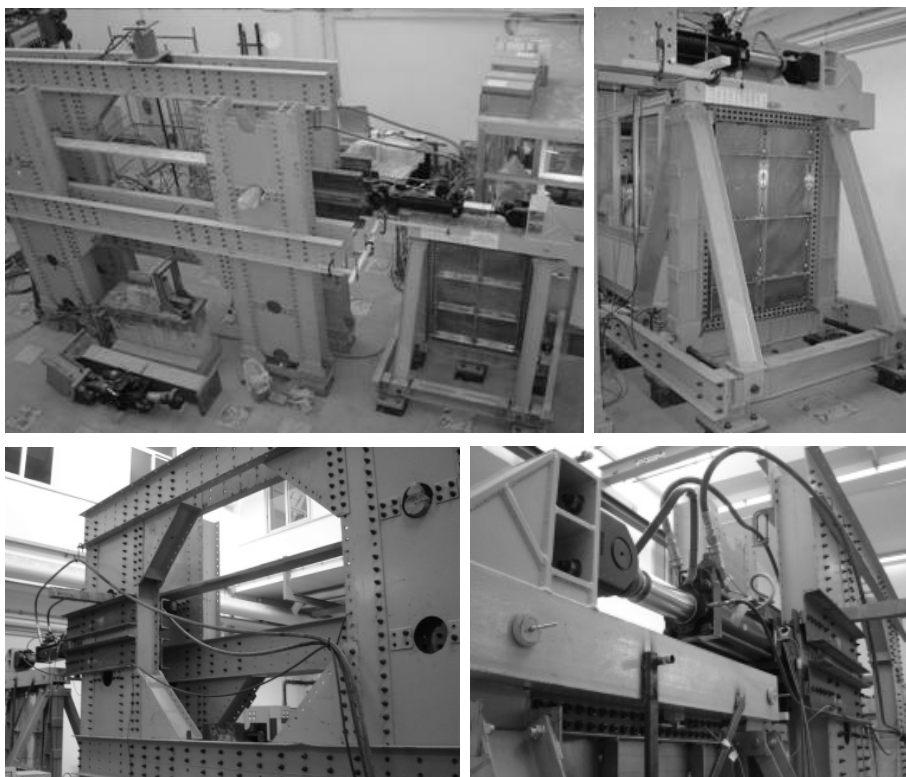


Figure 10. The testing equipment for the Full Bay type pure aluminium shear panels

(Fig. 9). More details on both the testing apparatus and layout, as well as means of measurements are provided in De Matteis et al. (2007^a).

The main results of these experimental tests have been represented by the relationship between the system reaction shear load and the applied lateral displacement (Fig. 11). For each specimen such a relationship has been normalized, considering the average shear stress τ applied on the horizontal panel side, considering a nominal cross-section $A = Bt = 5000 \text{ mm}^2$, and the equivalent shear strain γ , evaluated as ratio between the applied displacement and the panel nominal depth $H = 1500 \text{ mm}$.

It is important to observe that the considered shear strain comprises only the part related to the panel shear deformation, since the slips occurring in the panel connections as well the displacements of the reaction frame have been deducted from the global applied displacement.

The cyclic response of tested specimens has been interpreted by considering three numerical parameters characterising the behaviour of the system in terms of maximum

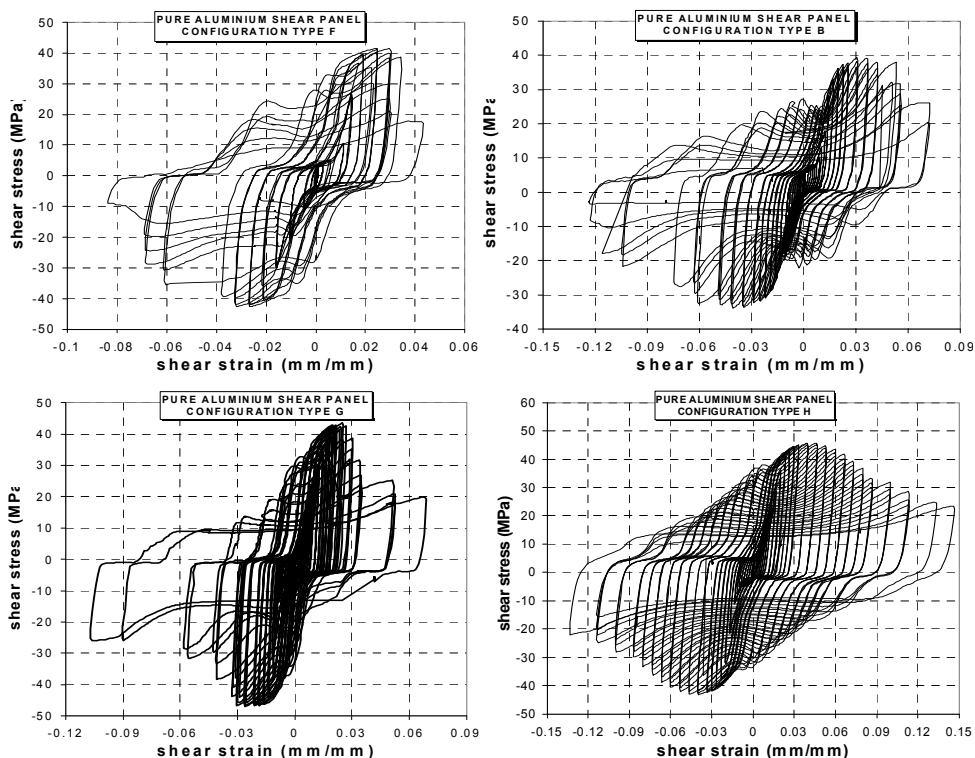


Figure 11. Hysteretic cycles provided by the tested full bay configurations

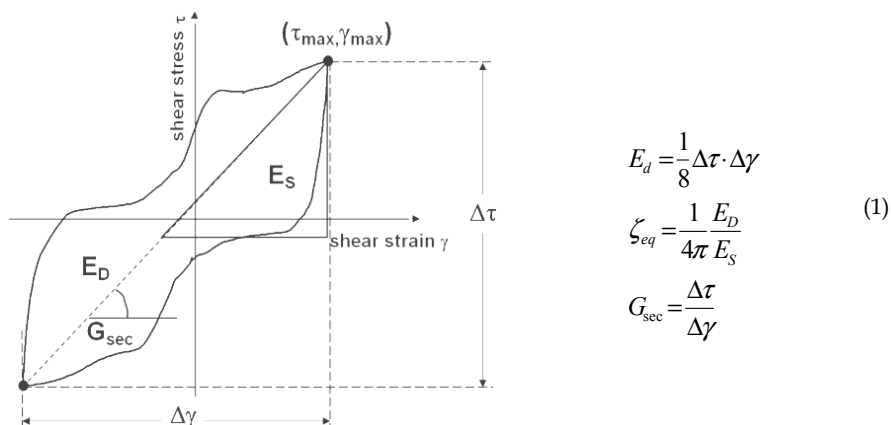


Figure 12. Definition of dissipated energy (E_d), equivalent viscous damping ratio (ζ_{eq}) and secant shear stiffness (G_{sec})

hardening ratio (τ_{max}/τ_{02} with $\tau_{02} = f_{02}/\sqrt{3}$), secant shear stiffness (G_{sec}) and equivalent viscous damping factor (ζ_{eq}), as defined in both Figure 12 and Equation (1).

The obtained results are shown in Figure 13 for panels type B and F, and Figure 14 for panel type G and H.

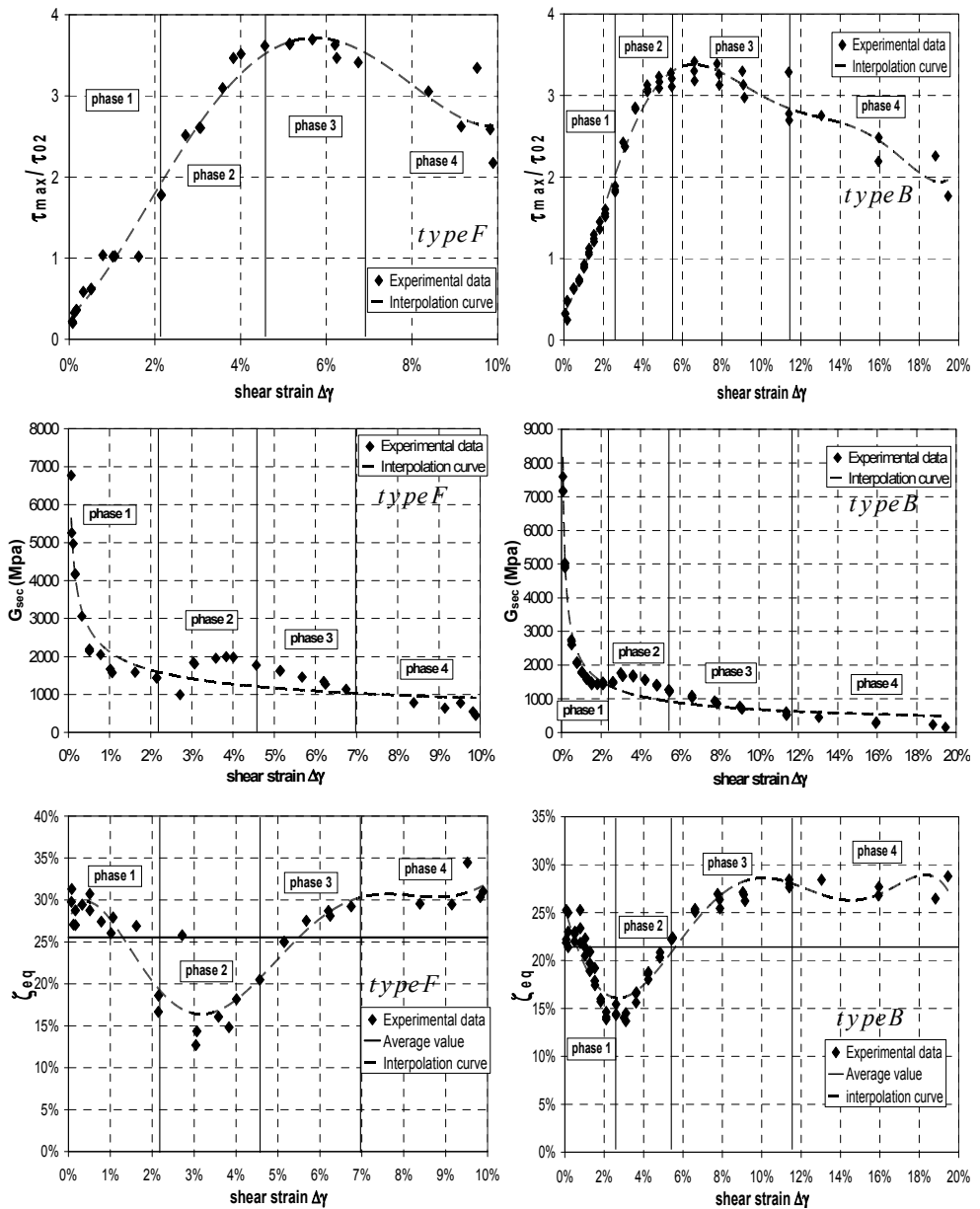


Figure 13. Cyclic performance of full bay shear panels type F and type B

In order to better emphasise the evolution of the system during the loading process, the cyclic behaviour of the tested panels has been furthermore divided in four different significant phases.

- phase 1: negligible buckling phenomena;
- phase 2: local buckling occurrence;
- phase 3: global buckling occurrence;
- phase 4: collapse phase.

These have been presented in more detail in [De Matteis et al., 2008^b]. As a further interpretation of panel behaviour, the relevant collapse modes for the tested panels were critically observed. These are depicted in Figure 15.

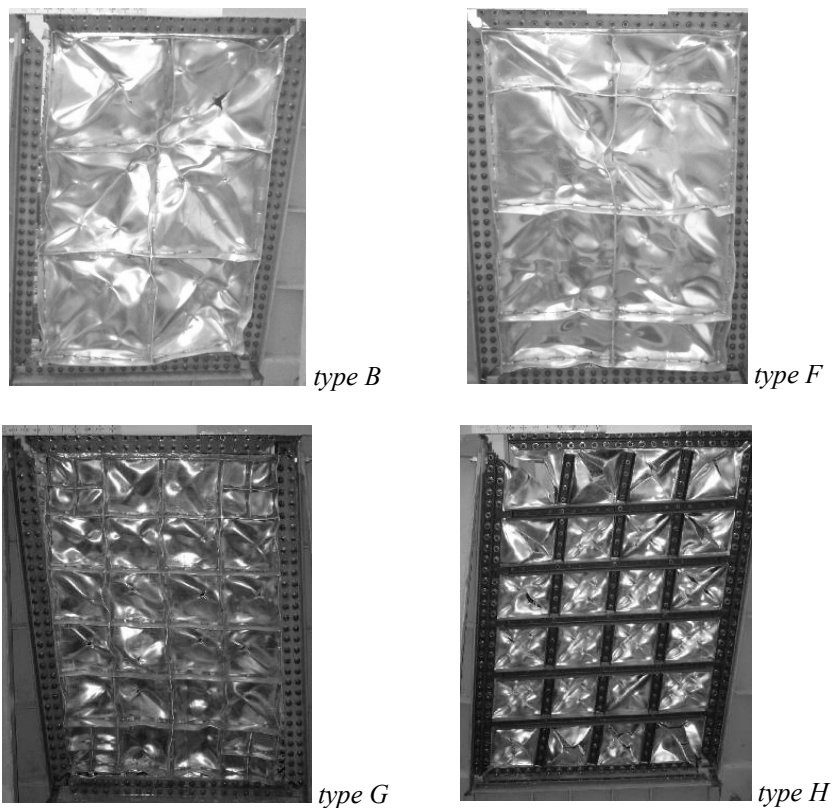


Figure 15. Collapse modes of the full bay panel typologies

3.2 Numerical analyses

Up to now, three of the above “full bay” shear panels have been numerically modelled, namely panel “type B”, “type F” and “type G”. For the first two panel types details are published in journal paper [De Matteis et al., 2008^c]; a parametrical analysis is provided in [Formisano et al., 2006]. A description of the panel “type G” numerical model is provided [De Matteis et al., 2007^d], and explained further in the present publication.

As it has been assumed also for the numerical modelling of “bracing type” shear panels (see Chapter 4.2) consistently to what is reported in [De Matteis et al., 2007^c], the proposed FEM model, implemented by the ABAQUS program (2004), reproduces the real geometry of the tested system by modelling the four arms of the perimeter steel frame with first order two-node three-dimensional B31 BEAM elements, while the four-nodes bilinear (with reduced integration and a large strain formulation) S4R SHELL finite elements, fixing five integration points through the thickness, have been used to model the aluminium sheeting and the applied stiffeners (Figure 16a). A side length of 25 mm has been considered for the adopted shell element mesh, this being the one that realizes the best compromise between accuracy of results and analysis time consuming (De Matteis et al. 2008^b). The beam elements have been constrained to each other by means of three-dimensional two-nodes hinged connector elements (type CONN3D2), while the whole external frame and the panel zones welded to the flange of the perimeter members have been restrained towards the out-of-plane deformations. The frame-to-panel connection, which is realized by means of tightened steel bolts located with a pitch of 50 mm, has been introduced in the model by considering that no slip between the different parts occurs. This has been modelled by using the TIE constraint of the ABAQUS program library, which has been applied between the panel edges and the corresponding frame members. Similarly, the same TIE command has been used to model the interaction between stiffeners and aluminium plate.

The geometrical imperfections of the system, mainly caused by the welded stiffeners, have been taken into account considering an initial deformed configuration, i.e. a combination between the buckling mode shapes corresponding to some of the first forty eigenvectors and assigning them a conservative maximum out-of-plane displacement of +5.00 mm, which represents a reasonable fraction of the free length involved in buckling phenomena. This large number of eigenvectors has been considered as the registered corresponding eigenvalues are really close to each other. However, among the above forty modes, only the ones which do not realize a superposition of deformed buckled shapes have been considered. For illustration, in Figures 16, two of the considered buckled deformed shapes,

corresponding respectively to the sixteenth (eigenvalue: 5144 N) and twenty-third modes (eigenvalue: 5417 N), are depicted.

The monotonic and cyclic behaviour of the base material has been modelled, in terms of true strain-true stress relationship, taking into account its actual non linear behaviour, according to the performed uniaxial tensile tests shown in Chapter 2.2, and considering the aforementioned cyclic hardening.

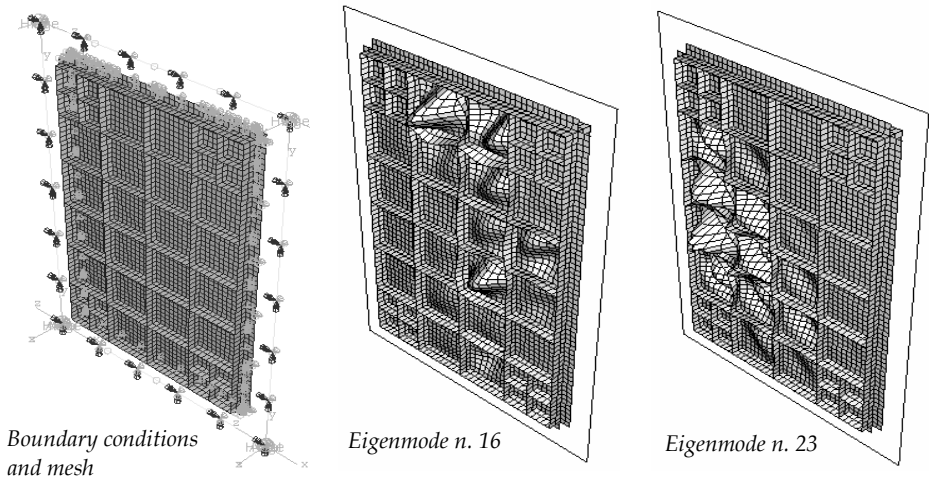


Figure 16. FEM model of the panel and typical eigenmodes (scale factor modes = 180)

The reliability of the above FEM numerical model has been checked using the available experimental results. In particular, in Figure 17a the comparison in terms of the global response is shown (cyclic response), evidencing the similarities of the obtained hysteretic cycles.

The numerical simulation has been carried out according to some of the most significant lateral displacements of the load history taken for the experimental tests, considering particularly the ones ranging from ± 12.5 mm to ± 70 mm. Behind the maximum threshold value, the occurred phenomena, namely the rupture of the perimeter connections which causes the reduction of the shear strength, have not been numerically reproduced. In Figures 17b -17d a detailed experimental-numerical comparison in terms of dissipated energy per cycle, secant global stiffness and equivalent viscous damping ratio is provided for the panel as a function of the applied shear displacement.

4 Analysis of bracing type shear panels

4.1 Experimental tests

Experimental tests on pure aluminium shear panels configured according to Figure 18 have been also carried out [De Matteis et al., 2009]. Tested specimens were characterized by global dimensions of 500 mm by 500 mm and thickness of 5 mm. As a consequence they presented slenderness ratio values a_w/t_w equal to 100 (BTPASP “type 1”), 25 (BTPASP “type 2”), 33 (BTPASP “type 3”) and 25 (BTPASP “type 4”) respectively.

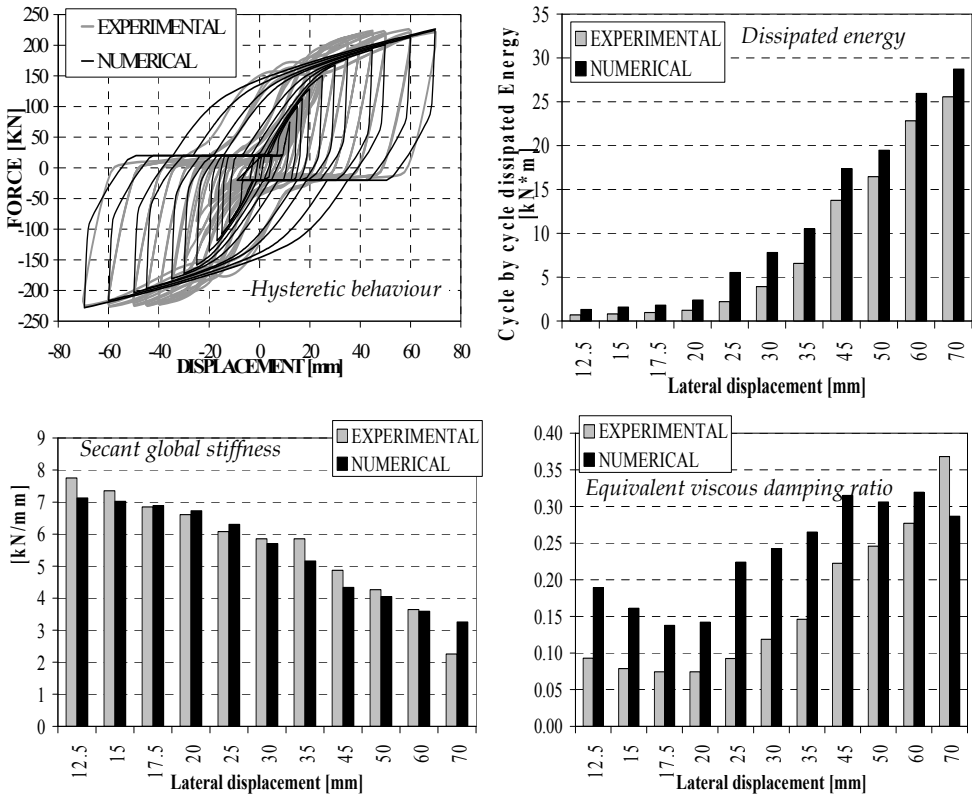
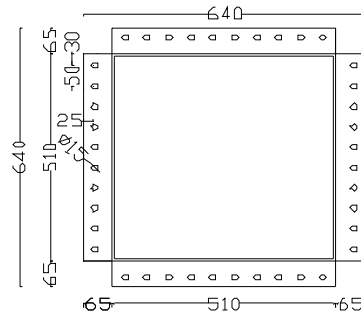
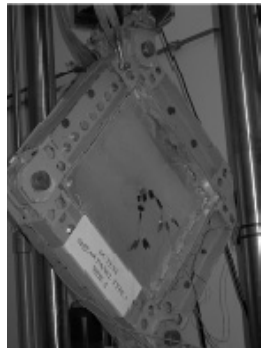


Figure 17: Comparison between numerical and experimental results

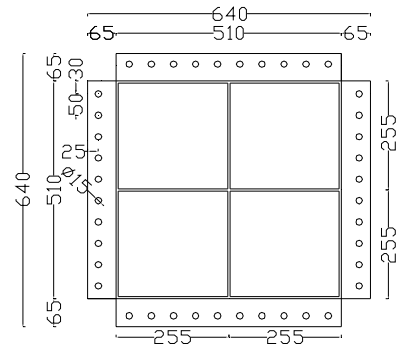
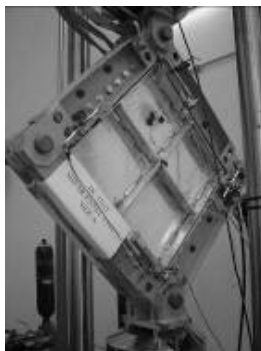
These values were obtained through the application of welded (MIG type) rectangular-shaped ribs. Such ribs were equally spaced on both faces of the panels, had a depth of 60 mm and were made of the same material and thickness of the base plates. Tested shear

panels were positioned into a square articulated steel frame made by four rigid built up members obtained by coupling two channel shaped profiles (Fig. 19a).

The aluminium plate was connected to steel profiles by means of 8.8 grade bolts having a diameter of 14 mm and a pitch of 50 mm. In particular, for each perimeter edge of the plate, eight internal bolts and two end bolts are present. Consequently, according to the EC9 provisions [2007] on connection strength, neglecting any partial factor, the shear bearing capacity can be assumed equal to 8.02 kN for outer bolts and 10.45 kN for each internal bolt. The steel frame was loaded by a MTS810 (Fig. 19b), with a maximum displacement of ± 75.0 mm and a maximum compression/tensile force of ± 500 kN. The diagonal displacement of tested panels was measured by a mechanical transducer whose signal was fed back in real time to the controller as an instrument of supervision of the jack motion. Also, four mechanical transducers were placed on the perimeter of the panels, to



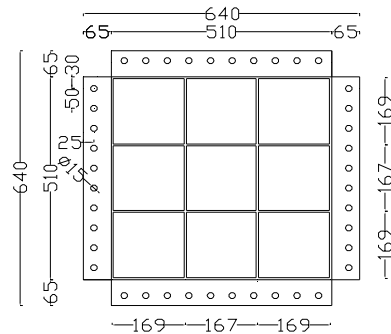
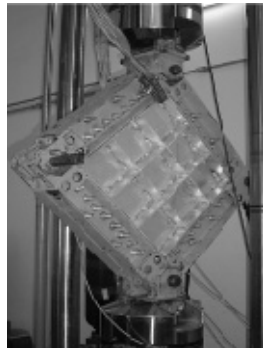
panel "type 1" ($a/tw=100$)



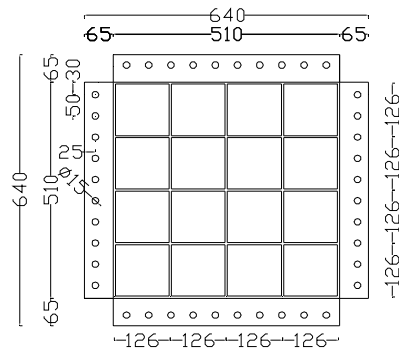
panel "type 2" ($a/tw=50$)

Figure 18. Tested specimens: bracing type shear panels (BTPASP)

measure the relative motion between the panel edge and the frame elements, in order to have the possibility to eliminate such an effect to assess the panel performance. To monitor the strain field of tested shear panels, a pair of uniaxial strain gauges were positioned at the centre of the panel for panel “type 1” and at the centre of a sub-panel of panel “type 2”, “type 3” and “type 4”. The applied measurement instrumentation and its arrangement and location can be observed in Figure 18. Tested specimens were subjected to diagonal cyclic forces, according to the displacement history shown in Figure 20. In Figure 21, the obtained hysteretic cycles for the tested specimens and in Figure 22 consistently with the definitions given in Figure 12, the cumulated dissipated energy and the equivalent viscous damping ratio are illustrated. These results clearly emphasize that the proposed panel configurations provided a good hysteretic performance, with large hysteretic cycles also for high deformation levels. Obviously the obtained results are influenced by different



panel “type 3” ($a/tw=33$)



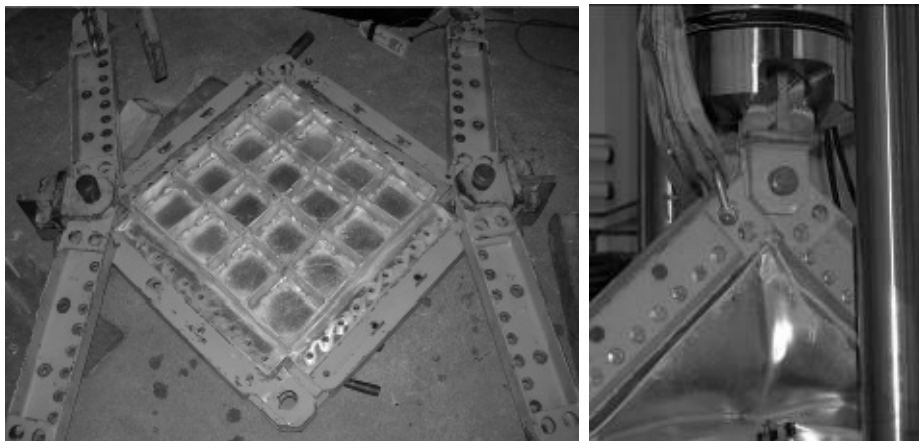
panel “type 4” ($a/tw=25$)

Figure 18. Continued

collapse modes depending on the applied stiffener configuration. In fact, in case of a lower slenderness ratio, the internal rib system acted as a sort of framework axially stressed, providing a resistant contribution to the panel, therefore transferring larger forces in the connecting system, which usually represents the weakest component of the studied devices. It is worth noticing that the higher values of the equivalent viscous damping factor (about 50%) were achieved for large shear strains which are compatible with the possible demanded shear strain during a severe earthquake.

4.2 FEM numerical models

In Figure 23, the four numerical models used the bracing type shear panels, calibrated in the same way of the full bay typology, are shown [De Matteis et al. 2008^b]. Also in this case,



a) Arrangement of the articulated perimeter steel frame b) Connection to the testing machine
Figure 19. Testing apparatus

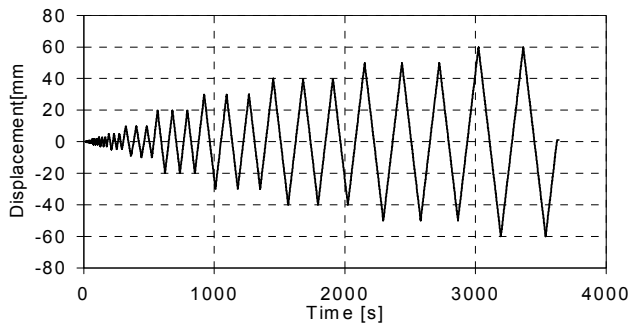


Figure 20. The displacement history on the tested specimens

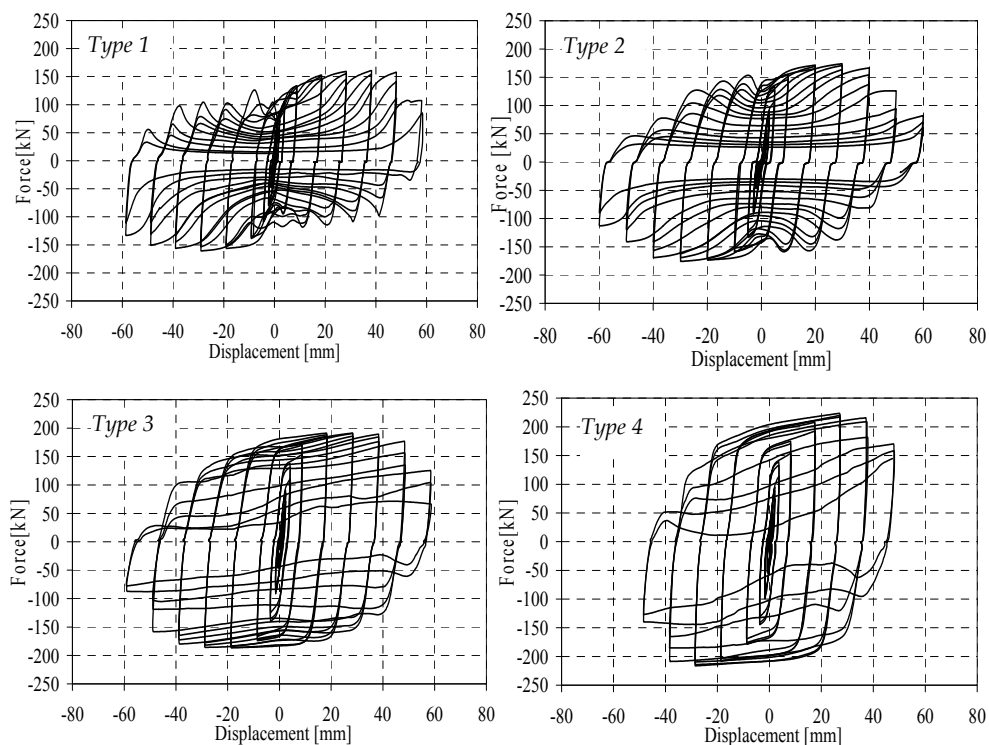


Figure 21. Hysteretic cycles

a mesh characterized by 25×25 mm elements has been adopted. In fact, by choosing 12.5×12.5 mm mesh elements, only a slightly higher accuracy could be achieved, whereas an increment of the analysis running time of 5 times resulted.

Geometrical imperfections have been taken into account by still considering a combination of eigenmodes and assigning to those a maximum out of plane displacement equal to $1/100$ of the free length of the panel portion detected by ribs for each panel.

In order to verify the reliability of the proposed numerical models, a comparison with the available experimental test results is shown. For this purpose, according to the experimental lay-out, an external diagonal displacement has been statically applied to the top beam of the external pin jointed frame of the FEM models. In Figure 24, the comparison is provided in terms of hysteretic cycles. It is to be noticed that only diagonal displacement demands ranging from -40 mm to $+40$ mm have been taken into account. In fact, when larger displacements are attained, the system response is influenced by both the failure of the perimeter connecting system and the fracture of the base plate, which are not

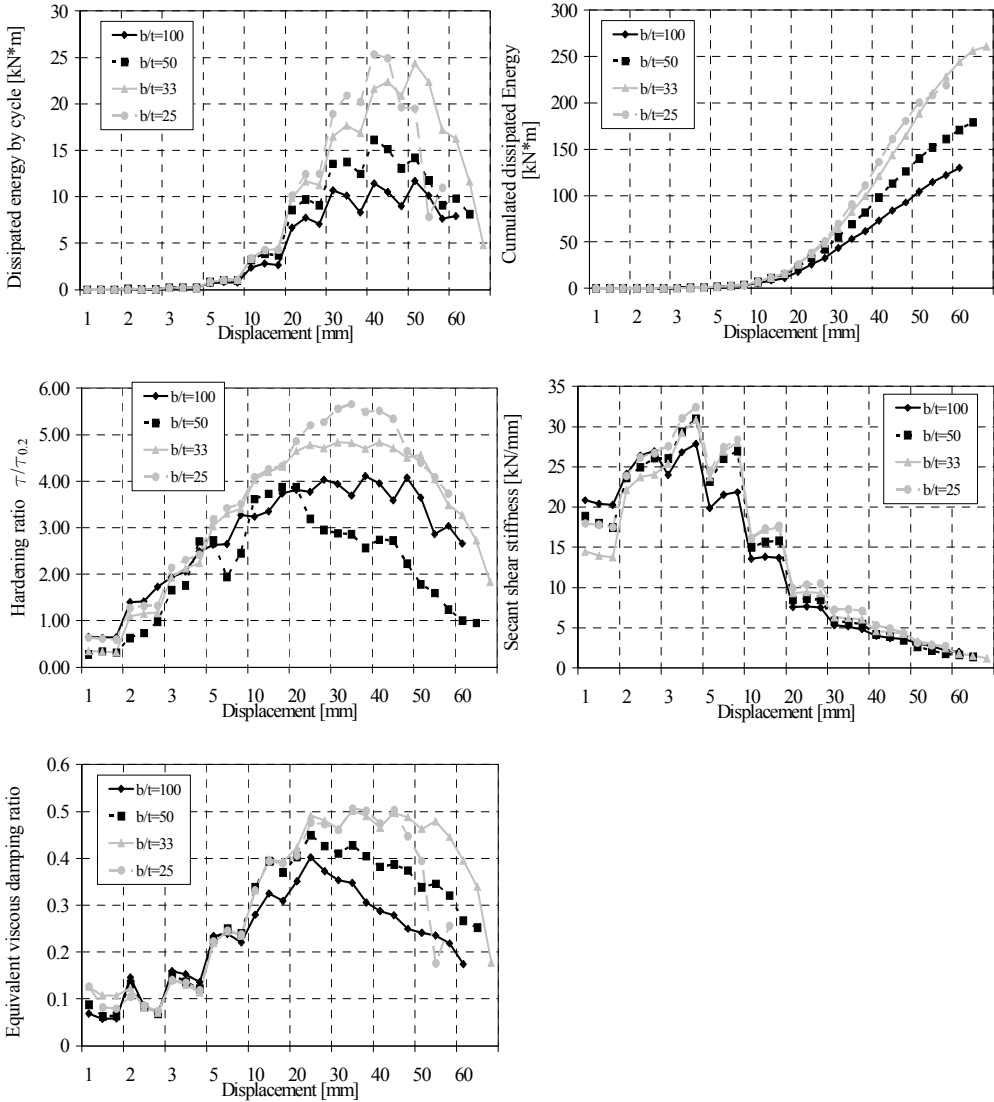


Figure 22. Experimental results

contemplated in the numerical model. These aspects are evident from a careful inspection of the experimental hysteretic loops from which it is possible to observe a contraction of the ± 40.0 mm second and third cycles. In Figure 25, the comparison in terms of secant stiffness is provided, while in Figure 26, the equivalent viscous damping measured at each shear strain demand is considered. The obtained results prove the reliability of the numerical model, which is able to capture all the main behavioural aspects of the system,

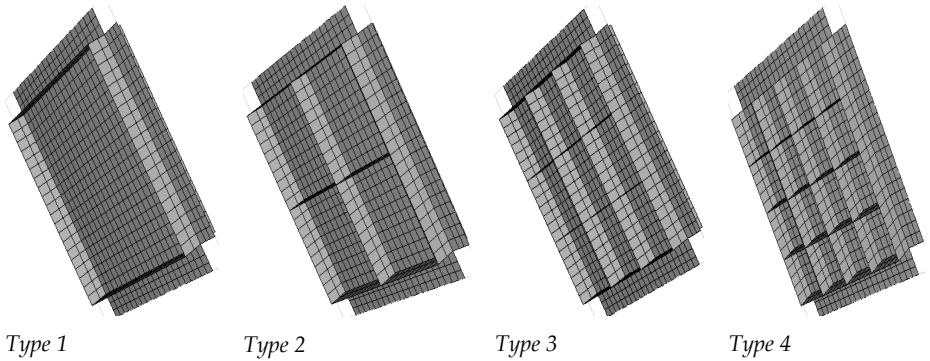


Figure 23. The FEM models

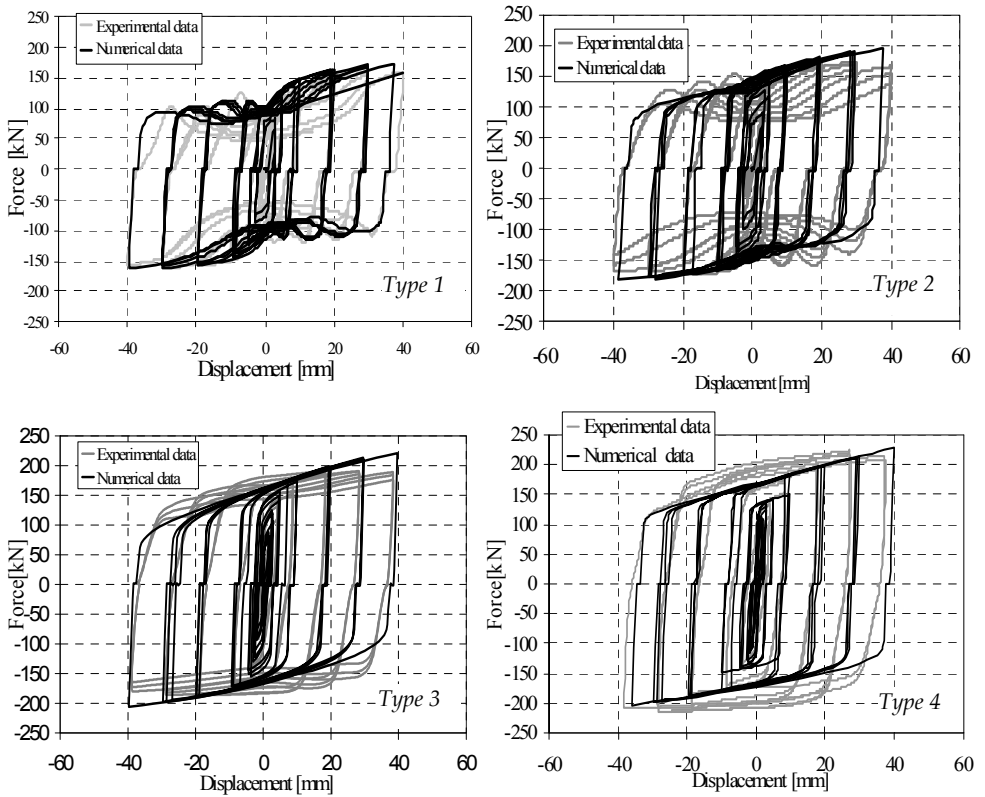


Figure 24. Comparison between numerical and experimental results in terms of hysteretic cycles

namely, the strength, the stiffness and dissipative features, including the pinching effects due to the buckling phenomena. It is also evident that the initial slipping phenomena, which are unavoidable for the practical tolerance in every steel structure and whose entity

has been interpreted during the calibration procedure of the numerical model, lead to a degradation of the dissipative response of the system for small displacement values. On the other hand, for medium-high shear deformation levels the dissipative capability reaches its maximum level, with peak values of the equivalent viscous damping factor of 40-45%.

Finally, in Figure 27 a comparison is also provided in terms of ultimate deformed shapes. For the sake of brevity only two of the four studied panels are shown. Also in this case, a good agreement between numerical and experimental results is recognizable. From the same picture, it is also possible to evidence the ultimate stress values.

4.3 Parametrical numerical analyses

Monotonic analyses have been carried out taking into account, for each of the above stiffened configuration, different slenderness values obtained by varying the panel thickness [Brando et al., 2009]. An increasing shear strain demand has been imposed and

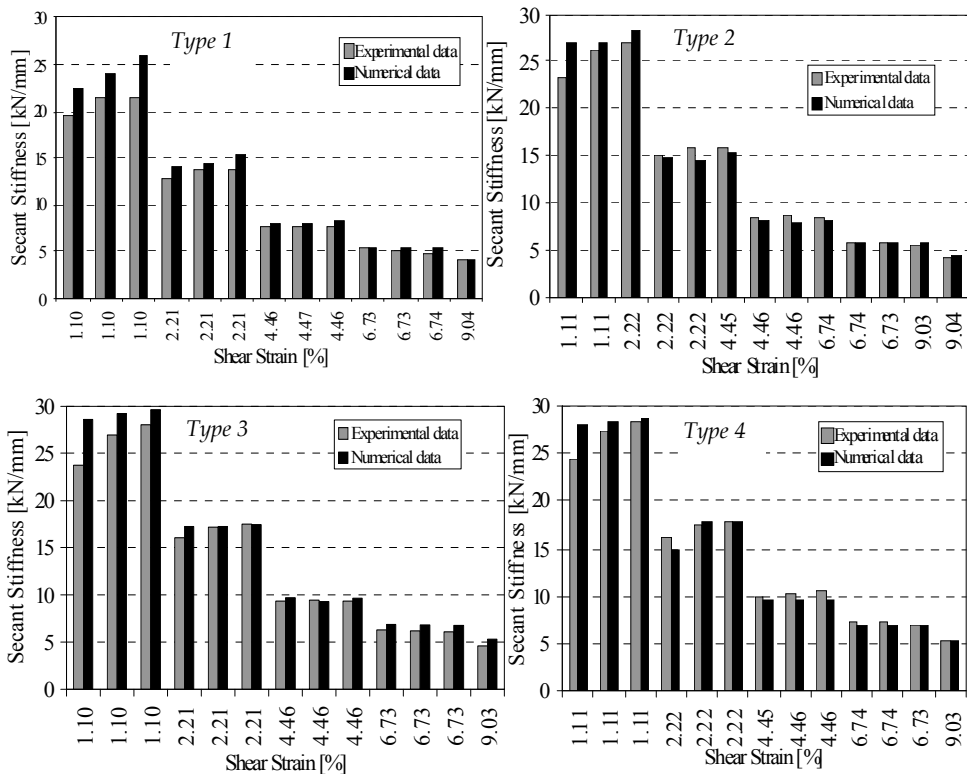


Figure 25. Comparison between numerical and experimental results in terms of secant stiffness

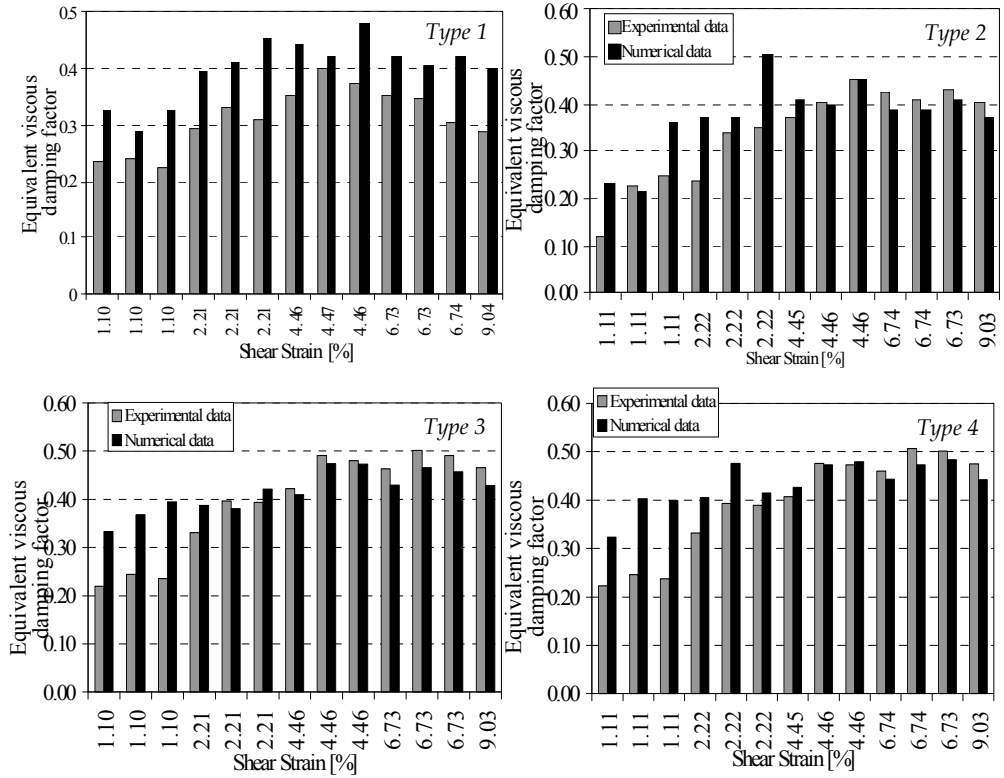


Figure 26. Comparison between numerical and experimental results in terms of secant stiffness

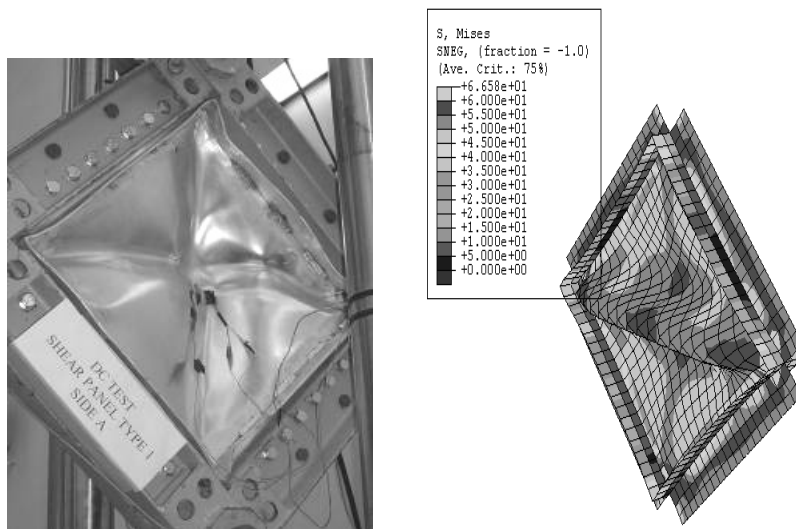


Figure 27a. Experimental and numerical ultimate deformed shapes of type 1

the shear force (V) versus shear strain (γ) relationships have been obtained. In this process, the failure of the base plate has been considered by assigning a softening branch to the base material true strain- true stress relationship. Moreover, no possible failure of the lateral connection system has been taken into account as these can be avoided by a correctly applied joint detail to be studied also on the basis of the aforementioned experimental and numerical studies. Then, the maximum shear strength for each panel thickness has been evaluated. In Figure 28 the factor for shear buckling ρ_v , evaluated according to eq (2) (in which t_w is the thickness of the web panel of the girder, h_w is the panel height, f_{0w} is the conventional yield strength of the web material, γ_{M1} is the safety factor) as the ratio between the measured maximum shear strength and the conventional

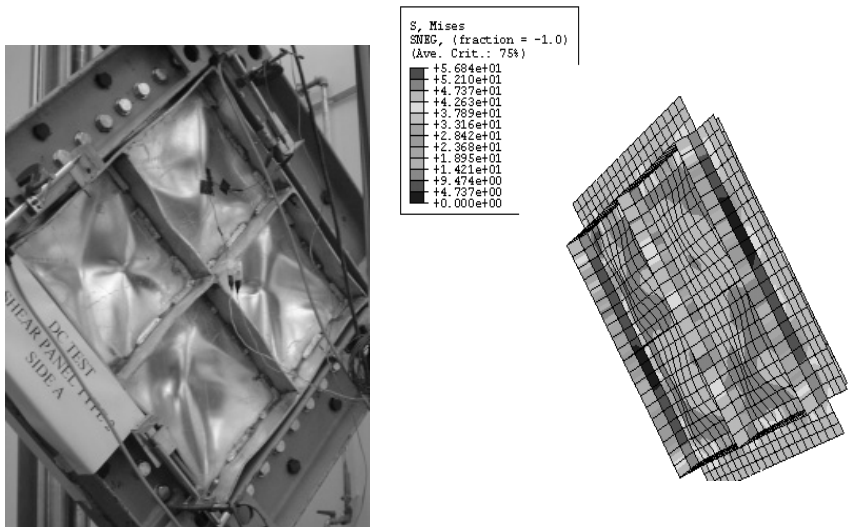


Figure 27b. Experimental and numerical ultimate deformed shapes of type 2

yield strength, is provided for different slenderness values λ_w , which have been defined consistently with definitions provided by Eurocode 9 [2007]. It is to be underlined that for multi-stiffened panels, the total shear strength has been reduced according to eq. (3), in order to take into account the contribution to the total shear strength given by the rib flexural stiffness.

$$V_{Rd} = \rho_v t_w h_w \frac{f_{0w}}{\sqrt{3} \gamma_{M1}} \quad (2)$$

$$V_{f,Rd} = \frac{b_f t_f^2 f_{0f}}{c \gamma_{M1}} \left(1 - \left(\frac{M_{ED}}{M_{f,Rd}} \right)^2 \right) \quad (3)$$

In this equation, b_f (not larger than $15 t_f$) and t_f are the width and thickness of the flange, f_{0f} is its yielding strength, c is provided by equation (4):

$$c = a \left(0.08 + \frac{4.4 b_f t_f^2 f_{0f}}{t_w b_w^2 f_{0w}} \right) \quad (4)$$

where a is the distances between the transversal ribs.

In Figure 28, the “first instability” curves have been plotted also. For each panel they

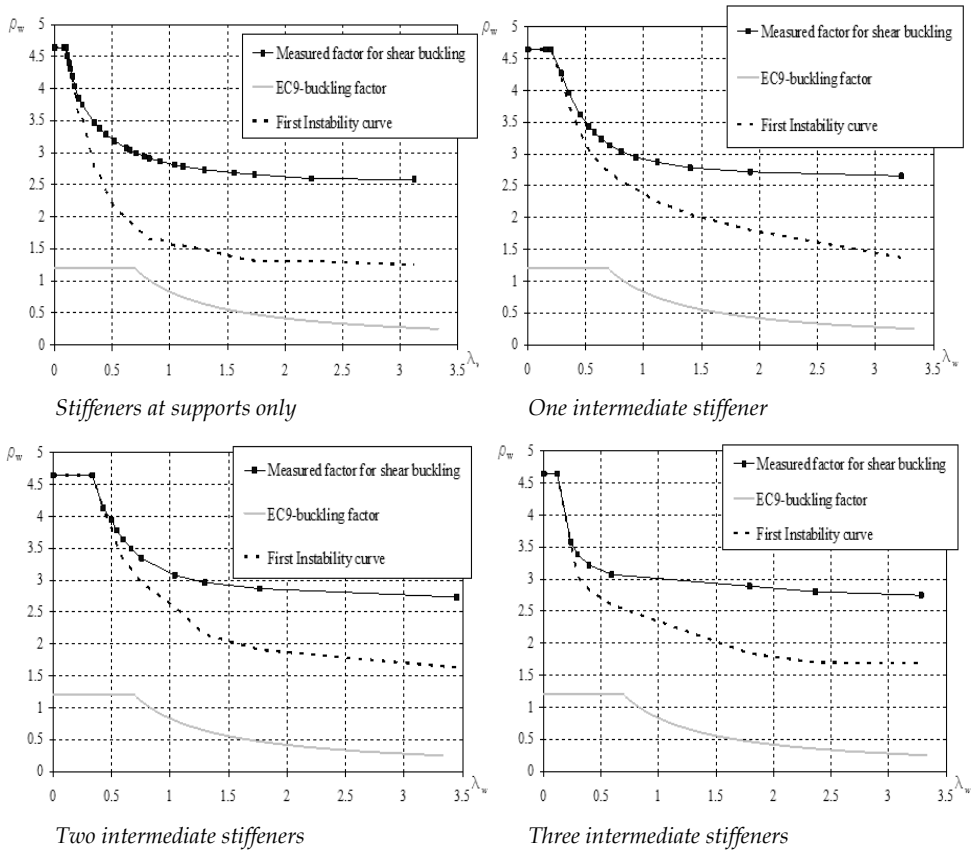


Figure 28. Shear buckling reduction factor for bracing type pure aluminium shear panels

represents the shear load corresponding to the occurrence of the first buckling phenomenon, normalized to the conventional elastic strength. This shear force has been detected for each slenderness value by measuring on the base plate the principal stress due to an increasing shear force and determining the value of these which corresponds to the arising of a tension field resisting mechanism, when the maximum compressive stress begins to be constant nevertheless the shear demand increases. Such a curve may represent an important design tool, allowing, for a given shear strength and/or shear deformation demand, the distinction between compact (for which the response of the system is not degraded by buckling phenomena) and slender shear panels.

In particular, width-to-thickness ratios of $(b_w/t_w)_1 = 16.6$, $(b_w/t_w)_2 = 33.3$, $(b_w/t_w)_3 = 62.5$ and $(b_w/t_w)_4 = 100$ have been detected as upper limits under which the studied panel typology may be classified as compact, independently by the shear strain value to which they are subjected, in the cases of panels with stiffeners at support, with one, two and three intermediate stiffeners respectively, are.

In addition, it is possible to observe that the proposed curves always provides values higher than 1, meaning that buckling phenomena develops after the conventional elastic strength of the material ($f_{0.2}$) has been attained.

5 Conclusions

A general review on the main results obtained by experimental tests and numerical models carried out for the assessment of the structural performance of stiffened pure aluminium shear panels have been provided in this paper. In a first stage, the material features, whose employment is really innovative in the structural engineering field, has been carried out. Experimental tests, results have allowed to put in evidence the convenience in using the proposed material for producing dissipative shear panels, because of its low yield stress, ductility and stable cyclic behaviour under both static and dynamic forces.

Therefore, two different shear panel configurations have been described. The first is based on a full bay configuration to be applied on frame structures by means of direct connections to beams and columns, whilst the former is conceived in a bracing type configuration and needs to be joined to the primary structure by means of auxiliary bracing elements. Tests under cyclic loading highlighted showed that the proposed devices could be effectively used as passive device for both steel and RC moment resisting frames, thank to the large energy dissipation capacity supplied, as has been testified by the peak value of the equivalent viscous damping ratio, which resulted to be around 50%.

Nevertheless, it has been put in evidence that bracing type pure aluminium shear panels are able to offer an highest performances for storey drift demands that are more commonly demanded to steel frames under high intensity earthquake (3% which corresponds to a diagonal displacement of 20-30mm). On the contrary, for the full bay typology the maximum dissipative capacity (measured by the equivalent viscous damping factor) is attained when storey drift demands of 6% - 8% occurs.

The results obtained by experimental tests have been also used in order to set up suitable numerical models able to interpret correctly the cyclic response of the system. The corresponding results have been employed to define appropriate shear buckling curves for proposed device, as a convenient design tool to be used for choosing the optimal panel configuration for determined shear strain demands.

Acknowledgments

This study has been developed in the framework of the Italian research project RELUIS. The authors are very grateful to Prof. Magnus Langseth and Dr. Raffaele Porcaro for their precious help in the implementation of the strain rate tests and their hospitality at the SIMLAB of Trondheim.

Literature

- ABAQUS Inc., 2004. "ABAQUS / Standard User Manual, Version 6.5". Providence, Rhode Island, USA; 2004.
- Baehre, R., 1966. "Trycktastravorav elastoplastikt material-nagrafragestallningar" ("Comparison between structural behaviour of elastoplastic material), Tekn. De Arne Johnson Ingenjorsbyra, Report No. 16.
- Brando, G., De Matteis, G., Mazzolani F.M.. "Design of Multi-stiffened Pure Aluminium Shear Panels for Passive Control devices", in Proceedings of the International Conference on "Protection of Historical Buildings" (Prohitech 2009), Rome, Italy, 21-24 June, F. M. Mazzolani editor, Taylor and Francis/Balkema publisher, London, ISBN-13: 978-0-415-55803-7, Vol. 1 pagg 663-668.
- Christopoulos, C., Filiatrault, A. "*Principles of Supplemental Damping and Seismic Isolation*" IUSS Press, Istituto Universitario di Studi Superiori di Pavia, Pavia, Italy, 500 p., 2006.
- De Matteis, G., Mazzolani, F.M., Panico, S.: "Pure aluminium shear panels as dissipative devices in moment-resisting steel frames". *Journal of Earthquake Engineering and Structural Dynamics*. June 2007^a; vol. 36, n. 7: pp. 841-859.
- De Matteis, G., Mazzolani F.M., Panico S., "Experimental tests on pure aluminium stiffened shear panels", *Engineering Structures*, DOI:10.1016/j.engstruct.2007b.11.015
- De Matteis, G., Brando, G., Panico, S., Mazzolani, F.M., "Numerical Analyses on Stiffened Bracing Type Pure Aluminium Shear Panels", in B.H.V. Topping, (Editor), "Proceedings of the Eleventh International Conference on Civil, Structural and Environmental Engineering Computing", Civil-Comp Press, Stirlingshire, UK, Paper 144, 2007^c. doi:10.4203/ccp.86.144 (web: <http://www.ctresources.info/ccp/paper.html?id=4527>)
- De Matteis, G., Brando, G., Formisano, A., Panico, S., Mazzolani, F.M., "Numerical and experimental study on pure aluminium shear panels with welded stiffeners". In *Advances in Steel Structures*, Proceedings of the 5th International Conference ICASS 2007 (Eds. JY Richard Liew, YS Choo), Singapore, 5 - 7 December 2007, CD-ROM, Vol. III, paper No. 106. ISBN:978-981-05-9371-1, published by Research Publishing Service.
- De Matteis, G., Brando, G., Panico, S., Mazzolani F.M.. "Pure Aluminium, an Innovative Material in Structural Engineering", Proceeding of the EUROSTEEL 2008 Conference, pp. 1885-1890, ISBN 92-0147-000-90, Graz, Austria, 03-05 September, 2008^a.

- De Matteis, G., Formisano, A., Panico, S., Mazzolani, F.M., "Numerical and experimental analysis of pure aluminium shear panels with welded stiffeners". *Computer and Structures*, 86 (2008^b) 545-555
- De Matteis, G., Formisano, A., Panico, S., Mazzolani, F.M., "Numerical and experimental analysis of pure aluminium shear panels with welded stiffeners". *Computer and Structures*, 86 (2008^c) 545-555
- De Matteis, G., Brando, G., Panico, S., Mazzolani F.M.. "Cyclic behaviour of Bracing Type Pure Aluminium Shear Panels (BTPASPs): Experimental and Numerical Analysis", Proceeding of the 14th. World Conference on Earthquake Engineering (14th WCEE), Beijing, China, 12-17 October, 2008^d. Paper ID: 05-06-0144 (Published on DVD)
- De Matteis, G. , Brando, G., Panico, S., Mazzolani, F.M., "Bracing type pure aluminium stiffened shear panels: an experimental study", in International Journal of Advanced Steel Construction (IJASC), S.L. Chan, W.F. Chen and R. Zandonini (editors-in-chief), ISSN 1816-112X, Vol. 5, No. 2, pp. 106-119 (2009)
- De Matteis, G. , Brando, G. , Mazzolani, F.M., "Mechanical Behaviour evaluation of pure aluminium by static and dynamic analysis", in Proceeding of Cost C-26 Conference, Mazzolani et al. Editors, Naples, 16th-18th 2010
- EUROCODE 9, (2007), "Design of Aluminium Structures", EN1999-1-1:2007
- Formisano, F. M. Mazzolani, G. Brando, G. De Matteis. "Numerical evaluation of the hysteretic performance of pure aluminium shear panels", in "Behaviour of Steel Structures in Seismic Areas" (STESSA 2006), F. M. Mazzolani and A. Wada editors, Taylor and Francis/Balkema publisher, London, ISBN 0-415-40824-5, 211-217.
- Nakashima, M., Iwai, S., Iwata, M., Takeuchi, T., Konomi, S., Akazawa, T., Saburi, K.: "Energy Dissipation Behaviour of Shear Panels Made of Low Yield Steel". *Earthquake Engineering and Structural Dynamics*, 1994, 23: 1299-1313.
- Ramberg, W. And Osgood, W.R., 1943. "Description of stress-strain curves by three parameters", NACA Techn. No.902.
- Pansieri, C., 1957. "Manuale di tecnologia delle leghe leggere da lavorazione plastica", Ulrico Hoepli editore, Milan, Italy.

